Micromachines **2010**, *1*, 19-33; doi:10.3390/mi1010019

OPEN ACCESS

micromachines

ISSN 2072-666X

www.mdpi.com/journal/micromachines

Article

Evaluation of Floor-grooved Micromixers Using Concentration-channel Length Profiles

Yan Du [1,2], Zhiyi Zhang [2,*], ChaeHo Yim [1], Min Lin [3] and Xudong Cao [1,*]

[1] Department of Chemical Engineering, University of Ottawa, Ottawa, ON K1N 6N5 Canada

[2] Institute for Microstructural Science, National Research Council Canada, Ottawa, ON K1A 0R6 Canada

[3] Canadian Food Inspection Agency, Ottawa Laboratory Fallowfield, Ottawa, ON K2H 8P9 Canada

* Author to whom correspondence should be addressed; E-Mails: zhiyi.zhang@nrc-cnrc.gc.ca (Z.Z.); xcao@eng.uottawa.ca (X.C.); Tel.: +1-613-993-4198 (Z.Z.); +1-613-562-5800-2097 (X.C.); Fax: +1-613-562-5172 (X.C.).

Received: 13 March 2010 / Accepted: 11 May 2010 / Published: 17 May 2010

Abstract: We evaluated the dynamic micromixing performances in slanted groove micromixers (SGM) and staggered herringbone micromixers (SHM) and quantitatively compared their differences using concentration *vs.* channel length profiles obtained from numerical stimulations. It is found that faster and finer mixing took place in the SHM and the chaotic mixing was more effective at locations closer to the grooves; in comparison, slower and coarser mixing occurred throughout the whole channel of the SGM. Subsequently, the concentration profile-based characterization method was demonstrated in hybrid floor-grooved micromixers to study the interaction of SGM and SHM.

Keywords: micromixer; numerical simulation; concentration profile; mixing completion length

---

1. Introduction

In recent years, microfluidic systems have attracted increasing research efforts and are widely used in chemical reactions and life sciences, such as chemical micro-synthesis, production of active pharmaceutical ingredients, and DNA hybridization [1–3]. In these applications, rapid mixing of fluids flowing through microchannels is very important for reactions to take place within these microchannels.

To achieve complete mixing within a reasonable time and on a microchannel length scale, many micromixing technologies have been developed [4,5]. Broadly, micromixers are classified into two categories, active and passive, in nature. The passive micromixers are more practical than active micromixers which generally require external energy supplies to agitate the fluids. In order to achieve efficient mixing, one can utilize geometrical shapes of the microchannel to passively achieve the chaotic behavior. For example, Liu *et al.* achieved chaotic mixing using a three-dimensional serpentine microchannel which was designed to cause chaotic advections. However this approach was only partially successful as high Reynolds numbers (*Re*) flow was required to create chaotic advections due to their relatively high inertia [6]. Subsequently, Park *et al.* improved the serpentine micromixer design with a novel F-shape mixing unit which is developed to enhance the vertical lamination by reducing cross-sectional area at the recombination region [7,8]. The improved serpentine laminating micromixer showed better mixing performance, particularly at low *Re* for channels with low aspect ratios due to three different mixing mechanisms: rotation, lamination, and chaotic advection. In addition, Johnson *et al.* [9,10] demonstrated a series of slanted wells on the microchannel floor to realize quick mixing by introducing transverse transportation of the fluids. Stroock *et al.* [11] studied the mixing in both staggered herringbone micromixers (SHM) and slanted groove micromixers (SGM) at low *Re* and showed that mixing could be enhanced by using herringbone shaped asymmetric structures on the floor of the channel. Two counter-rotating vortices were found in the channels of SHM in a study by Aubin *et al.* [12], in which a computational fluid dynamics (CFD) was also used for simulation. Kim *et al.* [13] presented a chaotic micromixer, in which chaotic mixing was achieved by periodic perturbation of a helical type of flow obtained by slanted grooves. Periodically inserted barriers along the channel wall in the micromixer imposed alternating velocity fields with periodic existence of a hyperbolic point, resulting in a chaotic mixing. Among all of the successfully developed micromixers, those with grooved surfaces in a channel floor, such as SGM and SHM, have attracted intensive research interests and found numerous applications because they are simple and inexpensive to fabricate.

To characterize the mixing performance of the micromixers in order to better understand and design more efficient micromixers for different applications, a number of techniques, both experimentally [14–18] and theoretically [12,19–28], have been employed. Particularly, CFD has been widely used to study the mixing behavior of micromixers in details. For example, Wang *et al.* [19] conducted 3-D flow analysis using a CFD package for microfluidics (MemCFD^{TM}) and showed a cross-section velocity field and streaklines of SGM. Hassell and Zimmernan [20] presented a computational study of the complex flow through a SHM using COMSOL, a finite element method based software, to elucidate the fluid flow within the channel and characterize the effect of the grooves at moving fluid across the channel. Kee and Gavriilidis [21] numerically evaluated mixing performance of the SHM at $Re = 0.001 - 10$, in which 3-D velocity field was obtained via COMSOL simulations, and particle tracking methods were used to quantify the mixing performance to avoid numerical diffusion problems. Recently, Williams and colleagues [22] used confocal microscopy and COMSOL modeling to develop and evaluate analytical models of mixing in the SHM. They concluded that mixing was only a function of Péclet number and downstream position in the mixer.

While useful, most of the current characterization methods are indirect, mainly qualitative and they do not give quantitative data, such as mixing lengths or mixing time scales. To overcome this problem,

Aubin and colleagues quantified mixing quality with spatial data statistics, maximum striation thickness and residence time analyses [23]. Recently, Lee and Voldman optimized micromixer design to enhance dielectrophoretic (DEP) microconcentrator performance and used trapped bead distribution along the channel to characterize mixings in pure SGM and hybrid SGM+HM (which has slanted grooves in the first half of the channel and centered herringbone grooves in the second half) [29]. However, mixers for DEP-based microcencentrator aimed at circulating particles, instead of mixing two particle populations. In a previous study, we proposed to use a concentration profile *vs.* channel length method to characterize and analyze micromixing in SGM [30]. We showed that this new method provided specific quantitative data to directly characterize the performance of a mixer of interest. In this paper, we further advance this quantitative method to evaluate and compare micromixing processes in both SGM and SHM. As we suspect that SGM and SHM enhance mixing performance due to different mechanisms, we also study the mixing performance of a hybrid floor-grooved micromixer—partially SGM and partially SHM patterned mixer—in an attempt to design more efficient micromixers.

2. Numerical Simulation

This work focused on the evaluation of mixing two different fluids of different concentrations within the microfluidic channels with grooved surface. The geometries of SGM and SHM used in this study are shown in Figure 1.

Figure 1. Geometries of SGM (a) and SHM (b) where the groove depth is varied from 5 to 40 μm.

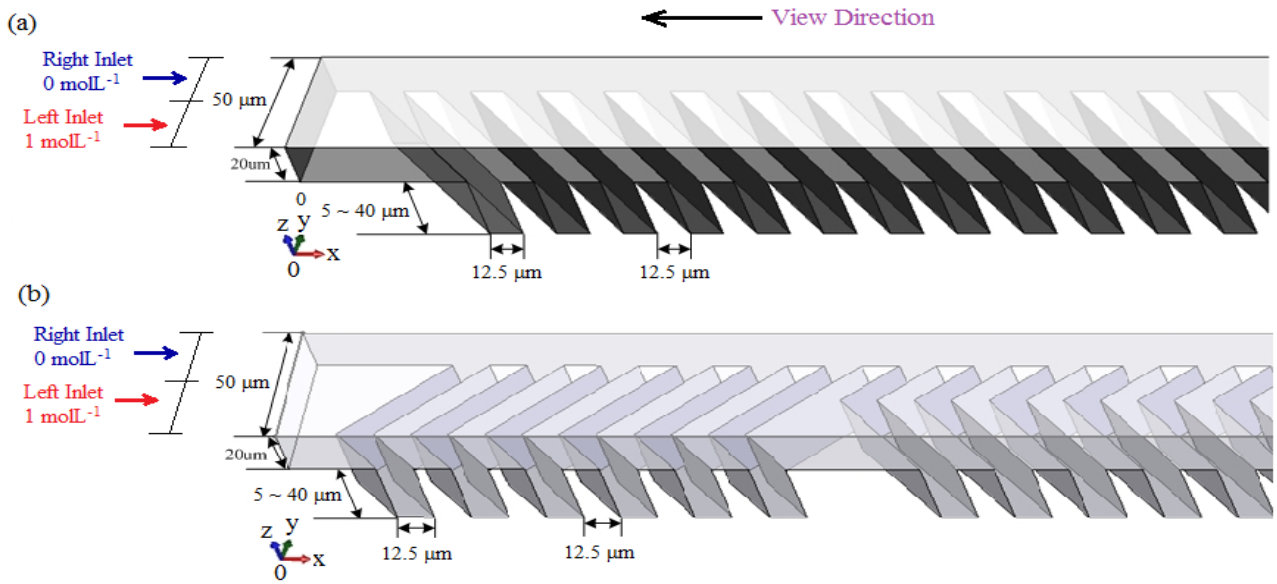

The microchannel cross-section dimension is 20 μm (height) × 50 μm (width); the groove width is 12.5 μm, and the groove depth is varied from 5 to 40 μm. The locations at which concentration data are collected are represented in the y–z coordinate system of the channel cross-section with its bottom-left set as origin (0, 0) (as seen in Figure 1). The total length of the simulated channel is 5 mm, which is the maximum allowable dimension for our targeted application. For the SHM, the grooves are

patterned at a 45° angle to the x-axis and the asymmetry index (fraction of the width of the channel occupied by the short arms of the herringbones) is one third, as suggested by Stroock *et al.* [11]. One half-cycle contains a group of six grooves, and the channel length occupied by one full-cycle is equal to 0.33 mm (cf. Figure 1).

The numerical simulation was to solve incompressible Navier-Stokes equations and convection-diffusion equations at steady state [28] using the CFD functions of COMSOL Multiphysics version 3.4 (Burlington, MA, USA).

Specifically, the two main equations to be solved are:

$$\text{Navier-Stokes equations: } \rho(\mathbf{u}\cdot\nabla)\mathbf{u} - \nabla\cdot\eta(\nabla\mathbf{u} + (\nabla\mathbf{u})^{\boldsymbol{T}}) + \nabla p = 0 \quad (1)$$

$$\nabla\cdot\mathbf{u} = 0 \quad \text{and}$$

$$\text{Convection-diffusion equation: } D\nabla^2 c - \mathbf{u}\cdot\nabla c = 0 \quad (2)$$

where ρ denotes fluid density (kg/m^3), **u** is the linear velocity of the fluid (m/s), η denotes viscosity of the fluid of interest (Pa·s), and p is the pressure (Pa), D denotes the diffusion coefficient (m^2/s) and c represents the concentration (mol/m^3).

This simulation was based on the finite element method (FEM), which uses free mesh elements that can easily adapt to the structure of the channel. All the implementation was done by the software with the type of equations and the boundary conditions to be defined by the operator. The tetrahedral free meshing method, with a maximum element size scaling factor at 0.2, an element growth rate at 1.3, a mesh curvature factor at 0.2, a mesh curvature cutoff at 0.001 and resolution of narrow region at 1, was used in the simulation. It combined a triangular grid system with a tetrahedral grid at the wall region to capture the gradient near the channel walls. There were 1.0×10^6 to 1.5×10^6 of tetrahedral elements and 1.4×10^5 to 1.8×10^5 of triangular elements involved in the simulation in which mesh was adjusted according to specific device structures and mixing conditions to obtain the required convergence at a reasonable computing time scale while maintaining the required accuracy. The inlet flows were set as laminar flows. The boundary conditions were set as follows: outflow gauge pressure of the channel as 0 Pa (p = 0), velocity of the flows at the channel walls as 0 m/s (u = 0), and respective fluid concentrations at two inlets as 1 mmol/L (left inlet) and 0 mmol/L (right inlet). Both fluids were composed of the same type of solute and solvent. Other parameters used in the simulation included 0.01 m/s for the average linear velocity of both fluids at the inlets, and 10^{-10} m^2/s for the molecular diffusion coefficient for the solute in the solvent. The corresponding Reynolds number $Re = l\rho\upsilon/\eta$ of the studied fluids was therefore calculated to be 0.3 assuming that the fluids were aqueous solutions with density $\rho = 10^3$ kg/m^3 and viscosity $\eta = 0.001$ Ns/m^2, respectively.

3. Results and Discussion

3.1. Comparisons between SGM and SHM

For simplicity of discussion, a specific micromixer is represented by the type of micromixer followed by the numerical value of its groove depth. For example, SGM 5 represents a SGM with groove depth at 5 μm, and SHM 10 represents a SHM with groove depth at 10 μm. To compare mixing processes in SGM and SHM, we first took SGM 10 and SHM 10 as examples.

In principle, concentration-based analysis is the most reliable method in studying molecular micromixing because every aspect of the mixing process, such as bulk advection and molecular diffusion, will eventually be reflected in changes in concentration. The velocity field in SGM and SHM, as shown in Figure 2, can be helpful to understand the concentration change in a microchannel. In a steady flow, the streamlines coincide with the particle traces and the velocity vectors are tangent to the streamlines at all points [19]. As seen from the cross-section streamlines in Figure 2(c) and (d), there is only one overall helical flow in the SGM while two helical flows exist in the SHM. This is in good agreement with other reports in literature [19,21]. Before mixing, the fluids at two inlets had concentrations of 1 mmol/L and 0 mmol/L, respectively. With the rotation motions of the helical flow caused by either one vortex in SGM or two vortices in SHM to transport mass (thus mixing two fluids of two concentrations to be mixed), two completely different concentration profiles within the channels would result. Therefore, as the vortex flows transport masses to be mixed within a cross section and along the channels—before the fluids are completely mixed—one can imagine that the concentration of a specific point within a cross section will be different (either higher or lower) from that of the same point but at another cross section along the channel. The oscillations appear in the concentration *vs*. channel length profiles.

To study the mixing mechanics in SGM and SHM, we compared their concentration profiles, as shown in Figure 3.

Figure 2. Streamlines of velocity fields in (a), (c) SGM and (b), (d) SHM. (a), (b), 3D view. (c), (d), y-z plane viewed from inlet.

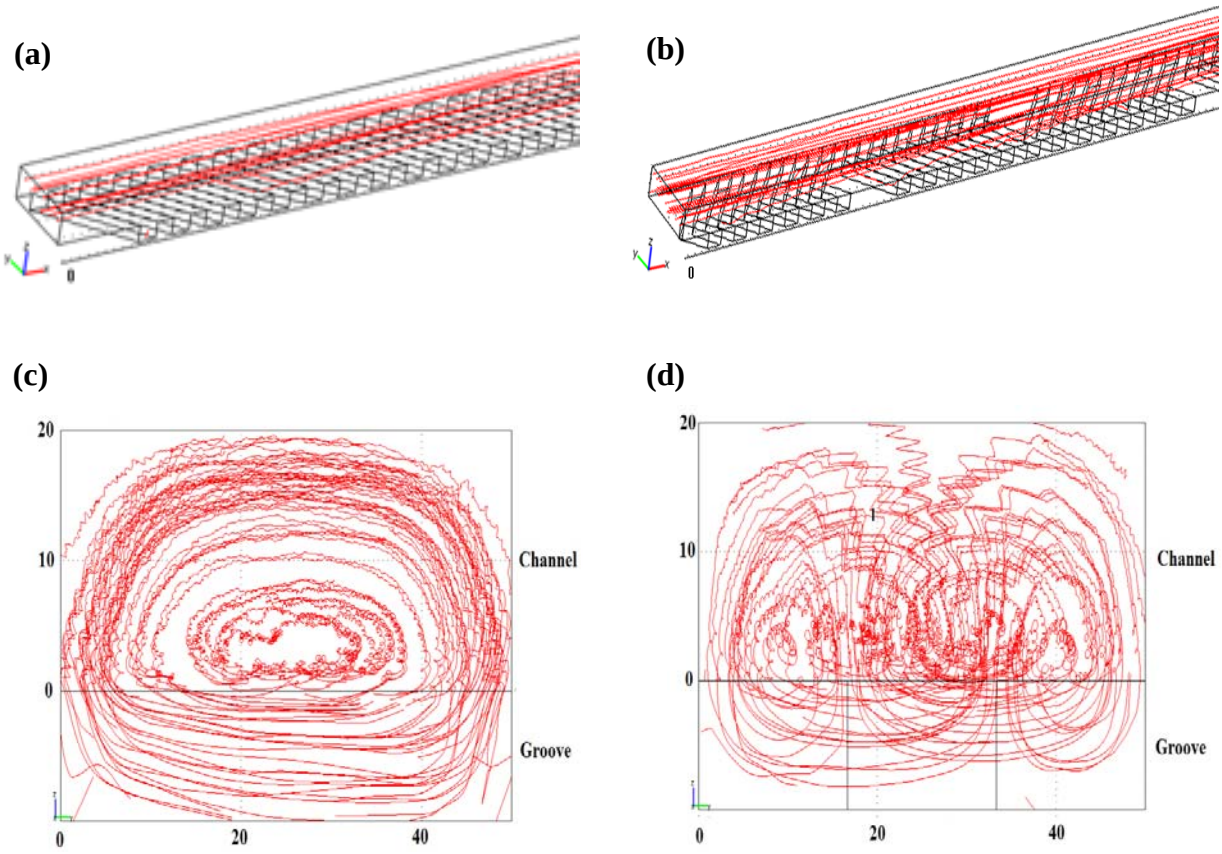

Figure 3. Concentration profiles within SGM 10 (a, c, e) and SHM 10 (b, d, f) along the channel length (in x-direction) (unit in mm). The concentration data were collected in the y–z coordinate system of the channel cross section with its bottom-left set as the origin (0, 0) (unit in μm). Channel dimension: 20 (h) × 50 (w) μm; groove dimension: 12.5 (w) × 10 (d) μm.

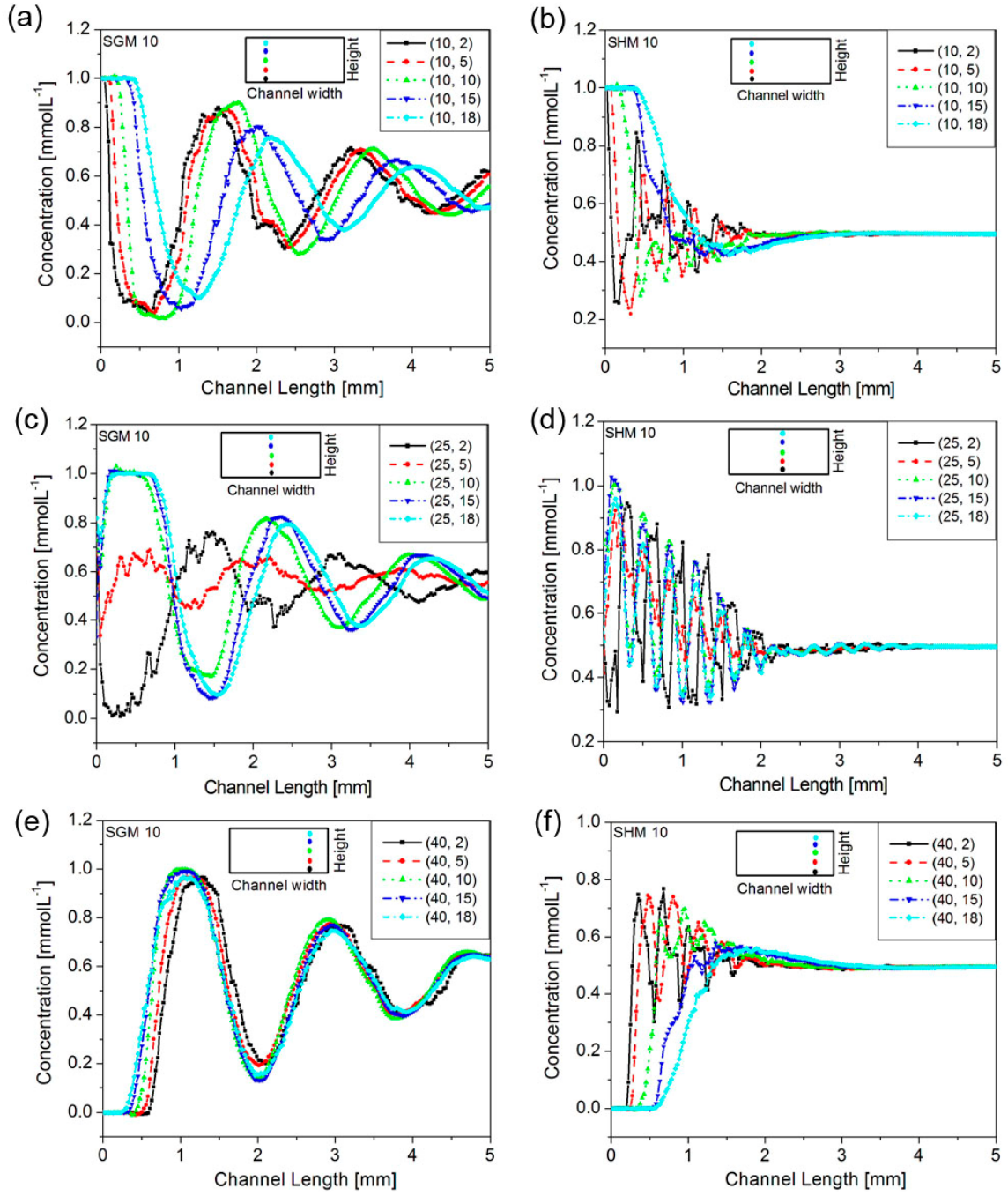

As generally discussed in the literature, a helical flow is created inside the microchannel of SGM due to a down-channel flow component as well as transversely rotational flow component [10,19,30]. All concentration profiles of SGM, as seen in Figures 3(a), (c) and (e), showed that the concentrations oscillated along the channel length as the two mixing fluids travelled helically and mixed along the channel length. In addition, these oscillations showed, in comparison with those in SHM, nearly the same amplitudes, larger peak-to-peak pitches and slower concentration convergences to the expected

concentration. This suggests that the single helical flow causes the concentration change at each cross-section location and that the overall mixing in SGM is coarse and slow. The concentration profiles collected at the middle of the SGM channel cross-section, as shown in Figure 3(c) were of particular interest. In this case, the concentrations at locations close to the grooves first decreased, likely due to the first arrival of low-concentration fluid from the right inlet (cf. Figure 1 for viewing directions); conversely, the concentrations at locations further away from the grooves first increased, likely due to the first arrival of high-concentration fluid from the left inlet. This observation further confirms that a clockwise (depending on the orientation of the grooves) helical flow is created in SGM mixers along the channel length to promote mixing. This is in good agreement with the results obtained by particle tracking method in the literature [19].

In the case of the SHM, one large clockwise vortex was created at long arms of the grooves, and one small counter-clockwise vortex was created at short arms of the grooves. These two transverse vortices changed periodically with the alternation of the asymmetry of structure and produced substantial oscillations and faster concentration convergence in the concentration profiles, as shown in Figures 3(b), (d) and (f). This clearly suggests that, in comparison with SGM, SHM enables finer (*i.e.*, more frequent) and faster mixing for the given flow rate investigated. Moreover, as seen from Figure 3(b) and Figure 3(f), the oscillations were more violent and with larger amplitudes at locations near the grooves; in contrast, the oscillations were delayed and less vigorous at locations further away from the grooves. These observations strongly indicate that the initial chaotic mixing in SHM is only limited to the regions close to the grooves until the upper portion of the channel fluid is sufficiently affected by the two opposing vortices. Since the two mixing fluids are first turned clockwise and then counter-clockwise by two vortices, the interface of two fluids (not the interface of two vortices) remains in the middle of the channel [12]. As the concentrations at the middle of the channel cross-section are always controlled by the large vortex, either left-positioned (high concentration) or right-positioned (low concentration), the concentration profiles at the middle of the channel cross-section, showed substantial oscillations at all times until mixing completed, as shown in Figure 3(d).

Since the groove depth has been shown to be one of the most effective parameters to affect mixing efficiency [31,32], we compared the effect of groove depth on the mixing performance in both SGM and SHM. As shown in Figure 4, the concentration data were collected at three different representative cross-section locations. At Location (1) which is near the grooves, all concentration profiles in both SGM and SHM showed increased initial slopes—concentration changed faster for a given mixing length in the channels—as groove depth increased from 5 μm to 30 μm, suggesting that mixing was significantly improved as the groove became deeper. This is in good agreement with a previously reported observation [25]. Comparing Figure 4(a) with Figure 4(b), it is evident that the concentration oscillations in the SHMs were more frequent than those in the SGMs and therefore the pitches of the SHM were much smaller than those of the SGM; this is likely a indication of a more active mixing in the SHM than in the SGM under the same fluidic conditions. As a result, the SHM demonstrated a significantly faster concentration convergence to the perfectly mixed value than the SGM at a given groove depth, as shown in Figures 4(a) and (b). This trend became more significant with increased groove depths. Likewise, the concentration profiles of the center-point of the mixers, both the SGM and the SHM, are shown in Figure 4(c) and Figure 4(d), respectively. As expected, the average pitches of SGM decreased with increasing groove depth, indicating more effective mixing efficiency due to

increased groove depth. Interestingly, pitches of the SHM remained the same regardless of the groove depth, and the pitch length was consistent with the channel length occupied by one full SHM structure cycle, indicating the full helical-flow cycle was *only* related to the structures in SHM. This observation was also noted in Figure 4(b). Like at Locations (1) and (2), similar mixing dependence on groove depth in SGM was observed at Location (3), a location further away from the grooves, as shown in Figure 4(e). However, in the case of SHM, as shown in Figure 4(f), the concentration streamlines showed small concentration oscillations before converging to the final concentration for all the groove depths investigated in this study. This strongly suggests that mixing by the two opposing vortices is less effective in the SHM at locations far away from the groove. This is in sharp contrast with the SGM of which the concentration streamlines showed less location dependence.

Nevertheless, based on the above discussion, we conclude that deep grooves are in favor of the chaotic mixing in both SGM and SHM and that the mixing is improved as the depth of the groove increases, as also described in previous reports [8,11,25].

From the concentration profiles, mixing completion length, L_m, can be easily calculated. Defined as the channel length needed to achieve a concentration value of $C = 0.5 \pm \varepsilon$ mol/L where ε is an assigned small value called mixing extent depending to specific application requirements. The L_m is the most straightforward parameter to characterize the mixing performance as a small L_m value corresponds to an efficient mixing.

We compared the effects of groove depth on the L_m at a specific $\varepsilon = 0.01$ for both SGM and SHM. As shown in Figure 5, both lines first fell sharply and then leveled off with further increased groove depths, indicating that deepening groove within a certain range was effective in enhancing the mixing, and any further increase in groove depth beyond a threshold was ineffective. More specifically, for SGM as shown of Line (1) of Figure 5, L_m values (while keeping $\varepsilon = 0.01$) decreased from 5 mm to 3.5 mm as the SGM groove depths increased from 20 μm to 30 μm. When the groove depths were further increased from 30 to 40 μm, the L_m remained almost constant at ~3.5 mm. For the SHM, as shown of Line (2) of Figure 5, mixing was significantly enhanced when groove depths were increased from 6 μm to 8 μm. However, when the SHM groove depths were further increased from 10 to 30 μm, the dependence of L_m on groove depth was insignificant. This result confirms the notion that a deeper groove does not always lead to a better mixing, as suggested by Aubin *et al.* who observed that a maximum groove depth existed whereby decrease in the maximum striation thickness was no longer significantly improved [23]. The reason for this to happen is that very deep grooves may also bring a significant negative contribution that would offset their positive effect on mixing. It is known that the groove-caused transverse fluid transportation within a microchannel simultaneously happens above the grooved floor and under the floor (*i.e.*, within the grooves). Those flowing above the floor are mostly in the vortices and experience a fast chaotic mixing, and those flowing within the grooves are basically in a typical laminar flow and are mostly exposed to a slow diffusion-dominated mixing. When the groove depth is overly increased, a large quantity of fluid enters the grooves and its slow mixing becomes significant to the overall mixing within the channel. The explanation is also in good agreement with the results reported in the literature that deep wells had a large dead volume which increased the residence time of the sample within the wells [10]. Furthermore, it is evident that at the same groove depth, a much smaller L_m value is needed for the SHM than the SGM, confirming that

mixing within the SHM is more effective and faster than that within the SGM. This is consistent with reported simulation and experimental results [11,12].

Figure 4. Concentration profiles in SGM (a, c, e) and SHM (b, d, f) with different groove depths. The concentration data were collected along channel length in its flow direction at the fixed cross-section locations represented by Location (1) at (5, 3) (coordinate units in μm), Location (2) at (25, 10), and Location (3) at (45, 17) in the y–z coordinate system of the channel cross section with its bottom-left point set as origin (0, 0). Channel dimension: 20 (h) μm × 50 (w) μm; groove width, 12.5 μm.

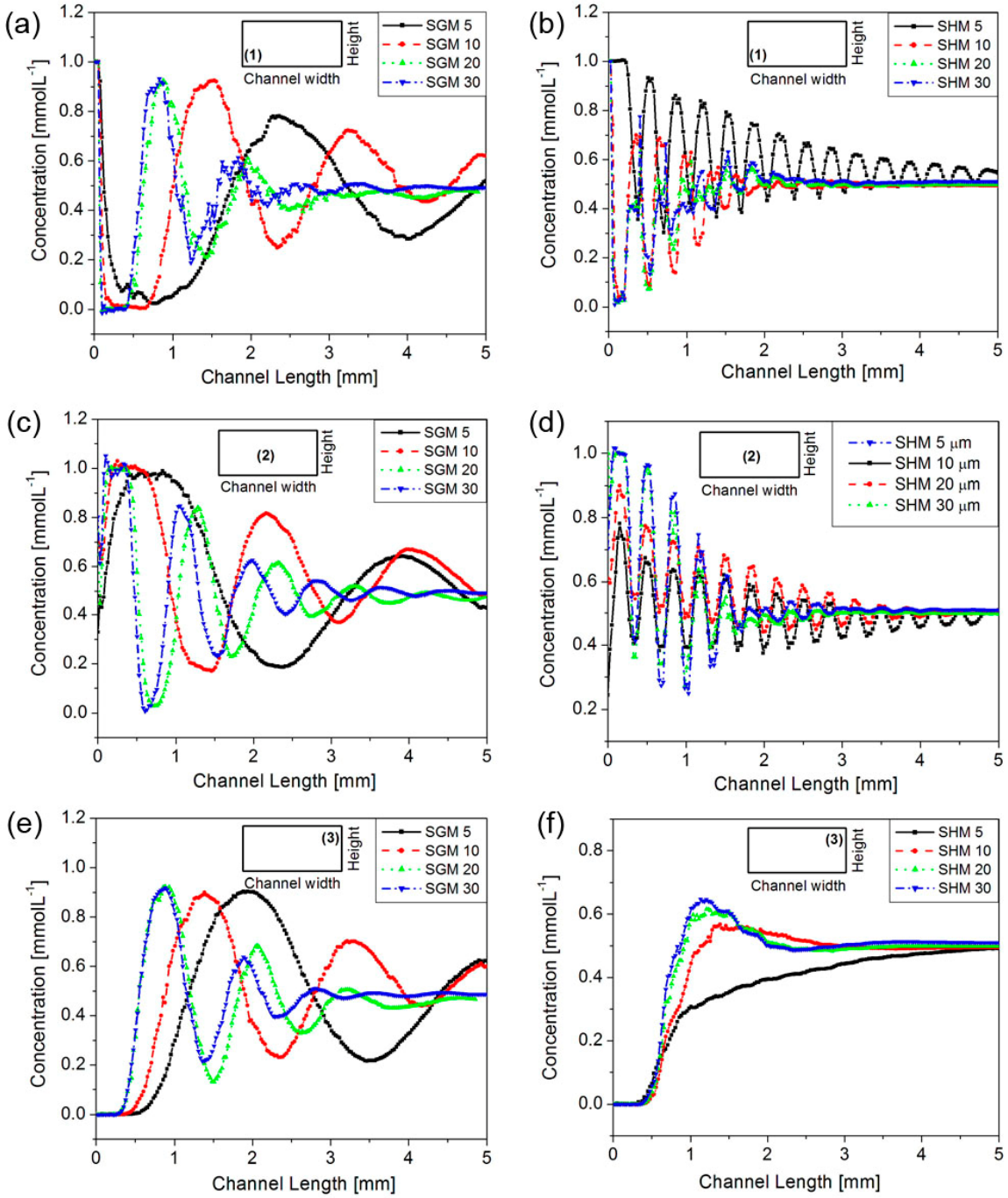

Figure 5. Effects of groove depths on L_m in SGM and SHM. Note that L_m simulation results did not converge for the mixing extent of ε = 0.01 within the simulated 5-mm channel length when the groove depths were less than 20 μm for SGM and 5 μm for SHM.

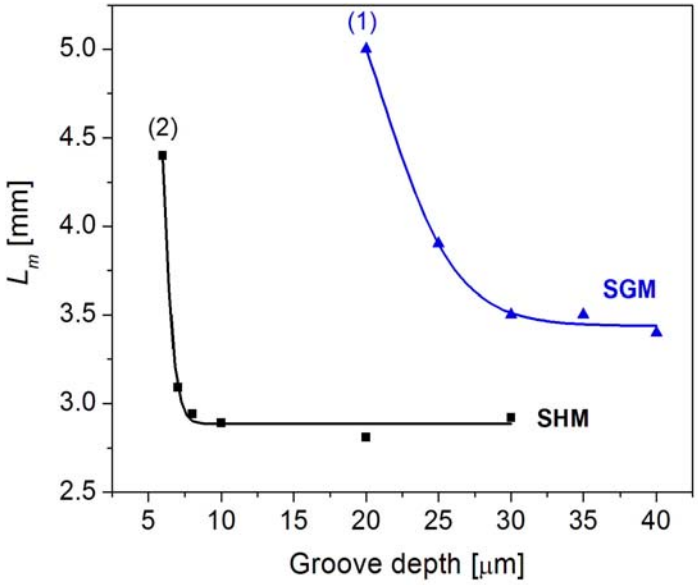

3.2. Hybrid floor-grooved micromixers

As has been clearly illustrated above, both the SGM and SHM mix different fluids via different mechanisms, and factors influencing their mixing efficiencies also work differently on the two different types of mixers. Therefore, in an attempt to design a more effective micromixer and to study the interactions between the SGM and the SHM, we designed hybrid floor-grooved micromixers of which two representative structures as examples are shown in Figure 6. Furthermore we quantitatively characterized and compared the micromixing in the hybrid floor-grooved micromixer using the concentration profile-based method as we have done earlier in this study.

Figure 6. The structures of hybrid floor-grooved micromixers: (a) SGM20+SHM; (b) SHM20+SGM. Channel dimension: 20 (h) × 50 (w) μm; groove dimension 12.5(w) × 20 (d) μm.

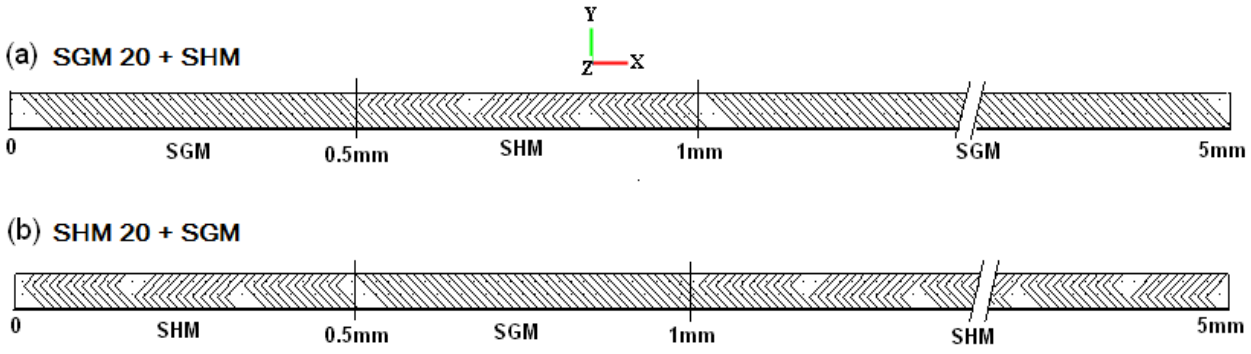

In comparison with the concentration profiles of SGM20, those of SGM20+SHM as shown in Figure 7(b) appeared to have more chaotic oscillations along the channel length from 0.5 to 1.5 mm. In

considering the location of the inserted SHM portion is from 0.5 mm to 1 mm, one should also note that oscillation inertia requires a certain distance along the channel to return to the original fluidic patterns as controlled by the slanted groove. This can be further confirmed by the mixing completion lengths L_m at different ε values. As seen from Table 1, for SGM20+SHM, an L_m value of 3.4 mm was needed at mixing extent of ε = 0.05, which was larger than 2.6 mm needed in a SGM20 only under same flow conditions. And yet, both of them achieved the mixing extent of ε = 0.01 at almost the same length, with respective L_m values of 4.6 and 4.7 mm. These results suggested that the mixing within SGM20+SHM did not improve mixing efficiency when a short staggered herringbone grooves segment was inserted into the slanted grooves.

Figure 7. Concentration profiles for (a) SGM20 and (b) SGM20+SHM. The concentration data were collected along channel length in its flow direction at the fixed cross-section locations represented with [1] at (5, 3) (unit in μm), [2] at (45, 3), [3] at (25, 10), [4] at (12.5, 15), [5] at (37.5, 17.5) in the y–z coordinate system of the channel cross section with its bottom-left point set as origin (0, 0). Channel: 20 (h) × 50 (w) μm; groove: 12.5 (w) × 20 (d) μm.

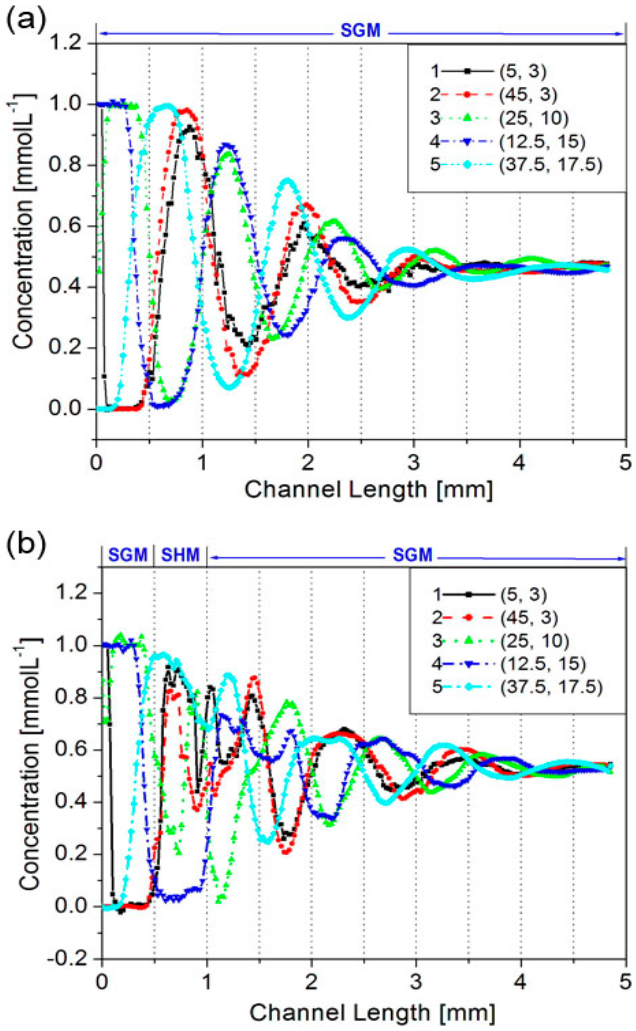

Conversely, we compared the concentration profiles of SHM20 and those of SHM20+SGM, which are shown in Figure 8. The concentration oscillations in SHM20+SGM became more complex and irregular along the channel length from 0.5 to 1.0 mm. Take Location (12.5, 15) as an example, its concentration oscillated violently along the channel occupied with slanted grooves and then showed two evident overshoots—one downward and one upward—which likely delayed the completion of mixing in the whole channel. Therefore, the resulting L_m in the SHM20+SGM was greater than that needed in SHM20, as shown in Table 1. This indicates a less efficient mixing within the SHM20+SGM.

Figure 8. Concentrations profiles for (a) SHM20 and (b) SHM20+SGM. Other conditions same as in Figure 7.

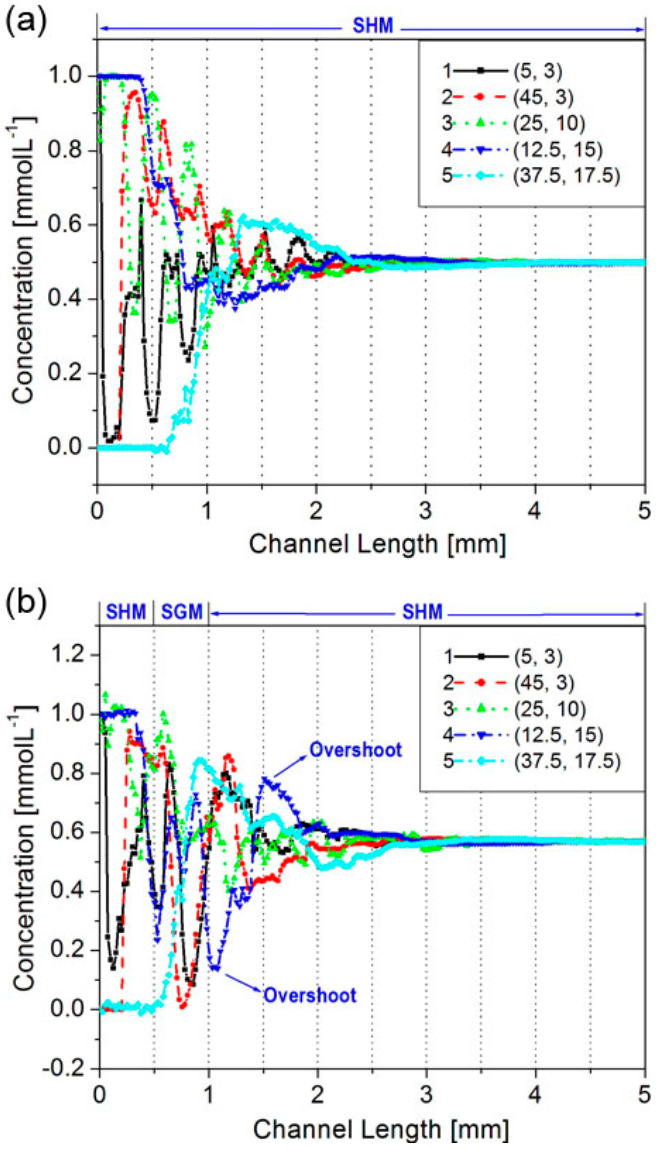

Furthermore, we calculated the L_m for the other hybrid floor-grooved micromixers with different groove depths or channel heights, and found that all of L_m values in hybrid floor-grooved micromixers were larger than those in the SGM and the SHM. This is probably because the interactions/transitions of the SGM and the SHM interfere the inherent oscillation of flow partners controlled by individual

SGM or SHM. As a result, a longer channel length is generally required for the oscillation to return to the original mixing patterns to achieve a complete mixing.

For many micromixing applications, it is important to characterize the mixing length, *i.e.*, L_m. While L_m doesn't provide detailed information about the mixing process, it is an essential performance parameter. Given that a significant research in the field of lab-on-a-chip is focused on various different applications, such a comprehensive performance parameter is useful for researchers to design specific micromixers. Therefore, the numerical method employed the current has two obvious advantages: (1) to directly reveal the detailed mixing process and (2) to provide a simple guide for a micromixer design in practical applications.

Table 1. L_m (in mm) for four micromixers at different ε values.

	$\varepsilon = 0.05$	$\varepsilon = 0.01$	$\varepsilon = 0.005$
(1) SGM 20	2.6	4.7	—[a]
(2) SGM 20+SHM	3.4	4.6	—[a]
(3) SHM 20	1.8	2.8	3.3
(4) SHM 20+SGM	2.1	3.1	3.7

[a] The concentration did not converge to 0.5 ± 0.005 mmol/L within the simulated 5-mm channel length and the corresponding channel length could not be calculated from the simulation results.

4. Conclusions

In conclusion, we evaluated and compared the detailed micromixing performance within the SGM and the SHM by the concentration profiles-based method. In the profiles for both SGM and SHM, the concentrations oscillated along the channel length as the two mixing fluids traveled helically and mixed along the channel length. However, the concentration oscillations caused by one helical flow in SGM showed the same amplitudes, larger peak-to-peak pitches and slower concentration convergences to the expected concentration, indicating the mixing was slower and coarser inside the whole channel of SGM. In comparison, the oscillations in SHM were caused by two transverse vortices changed periodically with the alternation of the asymmetry of structure and produced a faster and finer mixing in the SHM, especially the chaotic mixing was more effective at locations close to the grooves. For both SGM and SHM, deepening groove within a certain range was effective in enhancing the mixing, and any further increase in groove depth beyond a threshold was ineffective. Moreover, we studied for the first time the interactions between SGM and SHM in the hybrid floor-grooved micromixers and found that the mixing does not enhanced in the hybrid miromixer. The concentration profiles-based method has been demonstrated with two obvious advantages: to reveal directly the detailed mixing process and to provide a simple guide for a micromixer design in practical applications.

Acknowledgements

This study is supported by the Engineering Research Council of Canada (NSERC). The postdoctoral fellowship to Yan Du by the NSERC through a Strategic Grant is greatly appreciated.

References

1. Fukuyama, T.; Rahman, T.; Sato, M.; Ryu, I. Adventures in inner space: Microflow systems for practical organic synthesis. *Synlett* **2008**, *2*, 151–163.
2. LaPorte, T.L.; Wang, C. Continuous processes for the production of pharmaceutical intermediates and active pharmaceutical ingredients. *Curr. Opin. Drug Di. De.* **2007**, *10*, 738–745.
3. Das, T.; Chakraborty, S. Biomicrofluidics: Recent trends and future challenges. *Sadhana-Acad. P. Eng. S.* **2009**, *34*, 573–590.
4. Nguyen, N.T.; Wu, Z.G. Micromixers—A review. *J. Micromech. Microeng.* **2005**, *15*, R1–R16.
5. Hessel, V.; Lowe, H.; Schonfeld, F. Micromixers—A review on passive and active mixing principles. *Chem. Eng. Sci.* **2005**, *60*, 2479–2501.
6. Liu, R.H.; Stremler, M.A.; Sharp, K.V.; Olsen, M.G.; Santiago, J.G.; Adrian, R.J.; Aref, H.; Beebe, D.J. Passive mixing in a three-dimensional serpentine microchannel. *J. Microelectromech. Syst.* **2000**, *9*, 190–197.
7. Park, J.M.; Kim, D.S.; Kang, T.G.; Kwon, T.H. Improved serpentine laminating micromixer with enhanced local advection. *Microfluid. Nanofluid.* **2008**, *4*, 513–523.
8. Park, J.M.; Kwon, T.H. Numerical characterization of three-dimensional serpentine micromixers. *AIChE J.* **2008**, *54*, 1999–2008.
9. Johnson, T.J.; Ross, D.; Locascio, L.E. Rapid microfluidic mixing. *Anal. Chem.* **2002**, *74*, 45–51.
10. Johnson, T.J.; Locascio, L.E. Characterization and optimization of slanted well designs for microfluidic mixing under electroosmotic flow. *Lab Chip* **2002**, *2*, 135–140.
11. Stroock, A.D.; Dertinger, S.K.W.; Ajdari, A.; Mezic, I.; Stone, H.A.; Whitesides, G.M. Chaotic mixer for microchannels. *Science* **2002**, *295*, 647–651.
12. Aubin, J.; Fletcher, D.F.; Bertrand, J.; Xuereb, C. Characterization of the mixing quality in micromixers. *Chem. Eng. Technol.* **2003**, *26*, 1262–1270.
13. Kim, D.S.; Lee, S.W.; Kwon, T.H.; Lee, S.S. A barrier embedded chaotic micromixer. *J. Micromech. Microeng.* **2004**, *14*, 798–805.
14. Kling, K.; Mewes, D. Quantitative measurements of micro- and macro-mixing in a stirred vessel using planar laser-induced fluorescence. *J. Visualization* **2003**, *6*, 165–173.
15. Kling, K.; Mewes, D. Two-colour laser induced fluorescence for the quantification of micro- and macro-mixing in stirred vessels. *Chem. Eng. Sci.* **2004**, *59*, 1523–1528.
16. Panic, S.; Loebbecke, S.; Tuercke, T.; Antes, J.; Boskovic, D. Experimental approaches to a better understanding of mixing performance of microfluidic devices. *Chem. Eng. J.* **2004**, *101*, 409–419.
17. Bourne, J.R. Comments on the iodide/iodate method for characterizing micromixing. *Chem. Eng. J.* **2008**, *140*, 638–641.
18. Ohkawa, K.; Nakamoto, T.; Izuka, Y.; Hirata, Y.; Inoue, Y. Flow and mixing characteristics of sigma-type plate static mixer with splitting and inverse recombination. *Chem. Eng. Res. Des.* **2008**, *86*, 1447–1453.
19. Wang, H.Z.; Iovenitti, P.; Harvey, E.; Masood, S. Numerical investigation of mixing in microchannels with patterned grooves. *J. Micromech. Microeng.* **2003**, *13*, 801–808.
20. Hassell, D.G.; Zimmerman, W.B. Investigation of the convective motion through a staggered herringbone micromixer at low Reynolds number flow. *Chem. Eng. Sci.* **2006**, *61*, 2977–2985.

21. Kee, S.P.; Gavriilidis, A. Design and characterization of the staggered herringbone mixer. *Chem. Eng. J.* **2008**, *142*, 109–121.
22. Williams, M.S.; Longmuir, K.J.; Yager, P. A practical guide to the staggered herringbone mixer. *Lab Chip* **2008**, *8*, 1121–1129.
23. Aubin, J.; Fletcher, D.F.; Xuereb, C. Design of micromixers using CFD modelling. *Chem. Eng. Sci.* **2005**, *60*, 2503–2516.
24. Kang, T.G.; Kwon, T.H. Colored particle tracking method for mixing analysis of chaotic micromixers. *J. Micromech. Microeng.* **2004**, *14*, 891–899.
25. Liu, Y.Z.; Kim, B.J.; Sung, H.J. Two-fluid mixing in a microchannel. *Int. J. Heat Fluid F.* **2004**, *25*, 986–995.
26. Lynn, N.S.; Dandy, D.S. Geometrical optimization of helical flow in grooved micromixers. *Lab Chip* **2007**, *7*, 580–587.
27. Ansari, M.A.; Kim, K.Y. Application of the radial basis neural network to optimization of a micromixer. *Chem. Eng. Technol.* **2007**, *30*, 962–966.
28. Camesasca, M.; Manas-Zloczower, I.; Kaufman, M. Entropic characterization of mixing in microchannels. *J. Micromech. Microeng.* **2005**, *15*, 2038–2044.
29. Lee, H.Y.; Voldman, J. Optimizing micromixer design for enhancing dielectrophoretic microconcentrator performance. *Anal. Chem.* **2007**, *79*, 1833–1839.
30. Zhang, Z.Y.; Yim, C.H.; Lin, M.; Cao, X.D. Quantitative characterization of micromixing simulation. *Biomicrofluidics* **2008**, *2*, 034104–034112.
31. Yang, J.T.; Huang, K.J.; Lin, Y.C. Geometric effects on fluid mixing in passive grooved micromixers. *Lab Chip* **2005**, *5*, 1140–1147.
32. Ansari, M.A.; Kim, K.Y. Shape optimization of a micromixer with staggered herringbone groove. *Chem. Eng. Sci.* **2007**, *62*, 6687–6695.